The Astrophysical Journal, 619:L75–L78, 2005 January 20


# A COMPARATIVE STUDY OF THE SPATIAL DISTRIBUTION OF ULTRAVIOLET AND FAR-INFRARED FLUXES FROM M101

Cristina C. Popescu,[1] Richard J. Tuffs,[1] Barry F. Madore,[2,3] Armando Gil de Paz,[2] Heinrich J. Völk,[1] Tom Barlow,[4] Luciana Bianchi,[5] Yong-Ik Byun,[6] Jose Donas,[7] Karl Forster,[4] Peter G. Friedman,[4] Timothy M. Heckman,[8] Patrick N. Jelinsky,[9] Young-Wook Lee,[6] Roger F. Malina,[7] D. Christopher Martin,[4] Bruno Milliard,[7] Patrick Morrissey,[4] Susan G. Neff,[10] R. Michael Rich,[11] David Schiminovich,[4] Oswald H. W. Siegmund,[9] Todd Small,[4] Alex S. Szalay,[8] Barry Y. Welsh,[9] and Ted K. Wyder[4]

*Received 2004 April 16; accepted 2004 June 3; published 2005 January 17*

## ABSTRACT

The total ultraviolet (UV) flux (from 1412 to 2718 Å) of M101 is compared on a pixel-to-pixel basis with the total far-infrared (FIR) flux (from 60 to 170 $\mu$m) using the maps of the galaxy taken by the *Galaxy Evolution Explorer* (*GALEX*) in the near-UV and far-UV and by the *Infrared Space Observatory* (*ISO*) at 60, 100, and 170 $\mu$m. The main result of this investigation is the discovery of a tight dependence of the FIR/UV ratio on radius, with values monotonically decreasing from ~4 in the nuclear region to nearly zero toward the edge of the optical disk. Although the tightness of this dependence is in part attributable to resolution effects, the result is consistent with the presence of a large-scale distribution of diffuse dust having a face-on optical depth that decreases with radius and that dominates over the more localized variations in opacity between the arm and interarm regions. We also find a trend for the FIR/UV ratio of taking on higher values in the regions of diffuse interarm emission than in the spiral-arm regions, at a given radius. This is interpreted quantitatively in terms of the escape probability of UV photons from spiral arms and their subsequent scattering in the interarm regions, and in terms of the larger relative contribution of optical photons to the heating of the dust in the interarm regions.

*Subject headings*: dust, extinction — galaxies: individual (M101) — galaxies: spiral — infrared: galaxies — scattering — ultraviolet: galaxies

## 1. INTRODUCTION

It is not known to what extent the appearance of ultraviolet (UV) images of gas-rich star-forming galaxies differs from the intrinsic distribution of UV sources, because of the effects of absorption and scattering by dust grains. These effects can be quantified by a direct comparison of UV maps with maps of far-infrared (FIR) emission from the grains, since most of the absorbed UV light is reradiated in the FIR. Late-type face-on spiral galaxies are ideal for such studies, because a higher proportion of their bolometric output originates from the young stellar population emitting in the UV, and because the analysis is not complicated by inclination effects.

The nearly face-on Sc galaxy M101 was observed by *GALEX* (*Galaxy Evolution Explorer*; Martin et al. 2005) as part of the *GALEX* Nearby Galaxy Survey (NGS). The *GALEX* UV photometry of all discrete sources in M101 is presented by Bianchi et al. (2005). Here we compare the *GALEX* images of M101 with maps of this galaxy made using the ISOPHOT instrument (Lemke et al. 1996) onboard the *Infrared Space Observatory* (*ISO*). An alternative study of another galaxy from the NGS, M83, is presented by Boissier et al. (2005), who derive extinction radial profiles of that galaxy from *GALEX* UV imaging. Extinction radial profiles of a few spiral galaxies were also presented by Boissier et al. (2004) using FOCA and *IRAS* data. For statistical samples, Buat et al. (2005) have presented a complementary study of extinction based on *GALEX* and *IRAS* data. Studies of the stellar populations in the inner and outer disks of NGS galaxies are also presented by Thilker et al. (2005a, 2005b).

## 2. COMPARISON BETWEEN *GALEX* AND ISOPHOT IMAGES

*GALEX* observed M101 in its far-UV (FUV; 1530 Å) and near-UV (NUV; 2310 Å) bands (Morrissey et al. 2005). Using the *GALEX* pipeline, final images were produced with a spatial scale of 1.″5 pixel$^{-1}$. The point-spread function FWHM of the images were ~4″ and 5″ for the FUV and NUV bands, respectively. The ISOPHOT images were made in bands centered at 60, 100, and 170 $\mu$m, covering an overall spectral range from 40 to 240 $\mu$m. The FWHM of Gaussian beams having the same area as the ISOPHOT beams are 50.″5, 54.″5, and 107.″3 at 60, 100, and 170 $\mu$m, respectively. Details of the data analysis for the ISOPHOT observations of M101 are given in Tuffs & Gabriel (2003).

To compare the *GALEX* maps with the ISOPHOT maps, we converted the UV maps to the orientation, resolution, and sampling of the FIR maps. The UV images were convolved with the *ISO* beams and resampled every 15.″33 × 23.″00 for comparison with the 60 and 100 $\mu$m images, and every 30.″66 ×

[1] Max Planck Institut für Kernphysik, Saupfercheckweg 1, 69117 Heidelberg, Germany.
[2] Observatories of the Carnegie Institution of Washington, 813 Santa Barbara Street, Pasadena, 91101 CA.
[3] NASA/IPAC Extragalactic Database, 770 South Wilson Avenue, Pasadena, CA 91125.
[4] California Institute of Technology, MC 405-47, 1200 East California Boulevard, Pasadena, CA 91125.
[5] Center for Astrophysical Sciences, Johns Hopkins University, 3400 North Charles Street, Baltimore, MD 21218.
[6] Center for Space Astrophysics, Yonsei University, Seoul 120-749, Korea.
[7] Laboratoire d'Astrophysique de Marseille, BP 8, Traverse du Siphon, 13376 Marseille Cedex 12, France.
[8] Department of Physics and Astronomy, Johns Hopkins University, Homewood Campus, Baltimore, MD 21218.
[9] Space Sciences Laboratory, University of California at Berkeley, 601 Campbell Hall, Berkeley, CA 94720.
[10] Laboratory for Astronomy and Solar Physics, NASA Goddard Space Flight Center, Greenbelt, MD 20771.
[11] Department of Physics and Astronomy, University of California, Los Angeles, CA 90095.

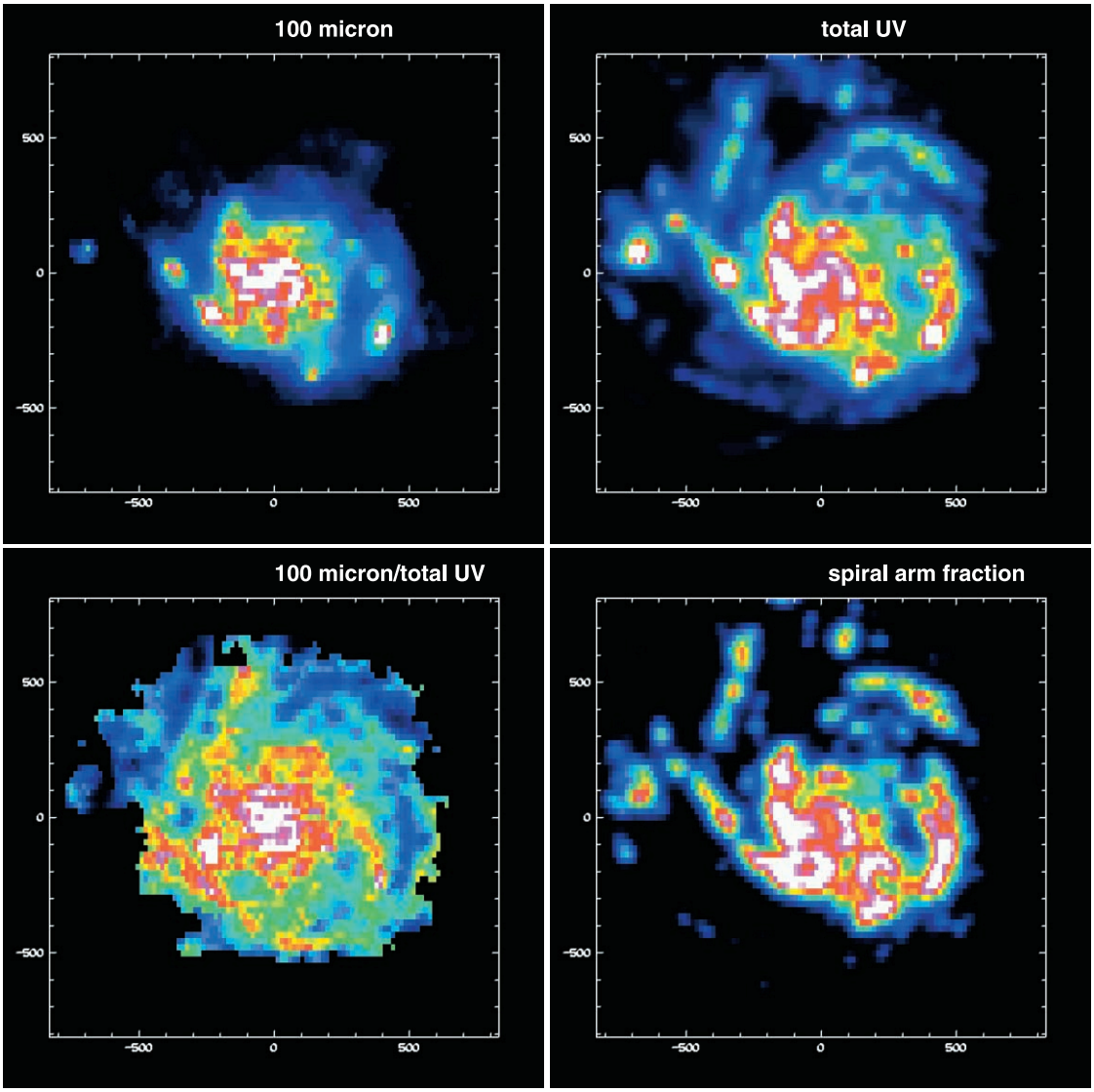


FIG. 1.—*Top left*: Filter-integrated 100 $\mu$m ISOPHOT image. The white color is for fluxes >0.50 × $10^{-14}$ W $m^{-2}$ $pixel^{-1}$, and the blue color has typical values of ~0.06 × $10^{-14}$ W $m^{-2}$ $pixel^{-1}$. The maximum flux is 1.38 × $10^{-14}$ W $m^{-2}$ $pixel^{-1}$. *Top right*: "Total UV" image converted to the orientation, resolution, and sampling of the 100 $\mu$m ISOPHOT image. The white color is for fluxes >0.39 × $10^{-14}$ W $m^{-2}$ $pixel^{-1}$, and the blue color has typical values of ~0.048 × $10^{-14}$ W $m^{-2}$ $pixel^{-1}$. The maximum flux is 1.03 × $10^{-14}$ W $m^{-2}$ $pixel^{-1}$. *Bottom left*: Ratio image of the filter-integrated 100 $\mu$m ISOPHOT image, divided by the corresponding "total UV" image. The white color is for ratios >1.49, and the blue color has typical values of ~0.17. The maximum ratio is 2.53. *Bottom right*: Image of the "spiral-arm fraction" at the orientation, resolution, and sampling of the 100 $\mu$m ISOPHOT image. The white color is for fractions >0.67, and the blue color has typical values of ~0.08. The maximum fraction is 1.00. All panels depict a field of 27′.7 × 27′.1 centered at $\alpha^{2000} = 14^h03^m13^s.11$, $\delta^{2000} = 54°21'06''.6$. The pixel size is 15″.33 × 23″.00.

92″.00 for comparison with the 170 $\mu$m image. The resulting images were corrected for Galactic extinction and then combined by means of a linear interpolation and integrated over wavelength to produce images of the UV flux integrated from 1412 to 2718 Å, calibrated in W $m^{-2}$. We refer to these combined images as "total UV" images, even though they do not contain the emission between 912 and 1412 Å and between 2718 Å and the *U* band. For a steady state star formation and a Salpeter initial mass function, we estimate that the factor needed to multiply the emission in the range 1412–2718 Å to obtain the true total UV emission is 1.95. This factor depends only to second order on the effects of reddening.

To facilitate a quantitative comparison between the "total UV" and FIR images, the ISOPHOT images were converted into units of W $m^{-2}$ by multiplying them by the corresponding filter widths. In the top panels of Figure 1, we display as an example the filter-integrated 100 $\mu$m ISOPHOT image (*left*), together with the corresponding "total UV" image (*right*). The 100 $\mu$m image appears smaller than the UV image, mainly because the FIR counterparts to the upper spiral arms prominent in the UV image are very faint at 100 $\mu$m. This effect is further quantified by the ratio image (100 $\mu$m/UV) displayed in the bottom left panel of Figure 1, where the region of the upper spiral arms coincides with low values of this ratio. At high surface brightness levels, however, the 100 $\mu$m and "total UV" images appear to trace similar structures. The prominent H II regions are seen in both direct UV light and in the dust reemission, albeit with varying ratios. The same is true for the general spiral structure. In addition, in both the 100 $\mu$m and "total UV" images, a diffuse emission underlies the spiral structure. In order to compare the 100 $\mu$m/UV color from the spiral structure with that from the underlying diffuse emission, we produced an image of the "spiral-

arm fraction," whose values give the fraction of the beam area occupied by spiral-arm structure. This was generated from the high-resolution UV image and is displayed in the bottom right panel of Figure 1. Comparison between the ratio image and the "spiral-arm fraction" image shows that the high values of the 100 $\mu$m/UV ratio trace the interarm regions. In other words, the "spiral features" in the ratio image are, in reality, regions of diffuse emission that are interspaced with the real spiral features, as seen in the "spiral-arm fraction" image.

## 3. THE RADIAL DEPENDENCE OF THE FIR/UV RATIO

A fundamental property of galaxies is the fraction of light from young stars that is reradiated by dust. With the advent of *GALEX* and FIR facilities like *ISO*, one can not only investigate this property for the spatially integrated emission (Xu & Buat 1995; Popescu & Tuffs 2002) but also as a function of position in the galaxy. To obtain a "total FIR" image, we combined the ISOPHOT 60, 100, and 170 $\mu$m images (at the resolution of the 170 $\mu$m image) by linearly interpolating between the bands and integrating over wavelength (between 60 and 170 $\mu$m), analogous to the procedure adopted to obtain the "total UV" image. As shown by Bothun & Rogers (1992), the dust in the inner regions of M101 is warmer than the dust in the outer regions, and there is considerable variation in the 60/100 $\mu$m ratio throughout the face of the galaxy, indicating a wide range of heating conditions. However, the FIR luminosity derived here is little influenced by dust temperature (or emissivity) variations, since the peak of all emission components from the warm and cold dust should lie within the broad spectral range of our filters (40–240 $\mu$m). The 170 $\mu$m band is particularly important in measuring the cold dust that accounts for most of the dust mass, as well as the bulk of the dust luminosity (Tuffs & Popescu 2003). The derived "total FIR" image still does not contain grain emission in the submillimeter and mid-infrared spectral ranges. Correcting for this spectral incompleteness in the same way as done by Popescu et al. (2002) for the late-type Virgo cluster galaxies observed by ISOPHOT (Tuffs et al. 2002) in the same filters as M101, we obtain a correction factor of about 2. This is comparable to the corresponding correction factor to convert fluxes in the "total UV" *GALEX* band into the true total UV fluxes. Thus, the ratio between the "total FIR" and "total UV" fluxes should be comparable to the ratio between the total flux from grains and the UV flux that would have been observed from 912 Å to the *U* band.

By dividing the "total FIR" image with the "total UV" image, we obtained a FIR/UV ratio map with a radial dependence as depicted in Figure 2. In the derivation of the radial distance, we neglected the small inclination ($i = 18°$; Sofue et al. 1997), since the value of the position angle is not well constrained and the effect on the result is very small. Figure 2 shows a remarkably tight dependence of the FIR/UV ratio on radius, with a monotonic decrease from values approaching 4 in the nuclear region to values approaching zero in the outermost regions. The tightness of the dependence is, presumably, at least in part an effect of the large beam, which averages the emission from sources of different FIR/UV colors. Nevertheless, some points of high-FIR/UV values emerge above the general trend between radii of 200″ and 500″. These points originate from an interarm region to the southeast of the nucleus. If these exceptional points are neglected, the radial variation of the FIR/UV ratio is well fitted by an offset exponential $f(r) = a(0) \exp[-r/a(1)] + a(2)$, with $a(0) = 3.98 \pm 0.19$, $a(1) = 360\farcs0 \pm 43\farcs7$, and $a(2) = -0.26 \pm 0.19$.

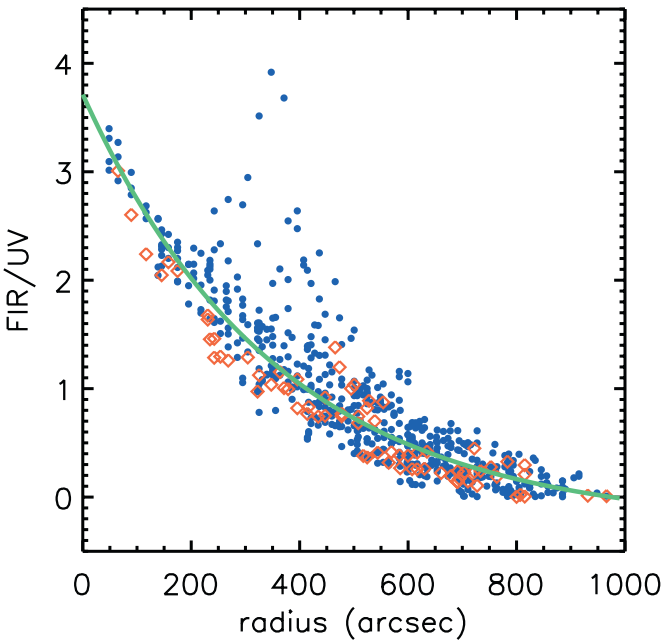


FIG. 2.—Pixel values of the FIR/UV ratio map at the resolution of the 170 $\mu$m image vs. angular radius. The blue dots are for lines of sight toward interarm regions, and the red diamonds toward the spiral arm regions. The green solid line is an offset exponential fit to the data.

Clearly, the major factor determining the FIR/UV ratio is radial position. To statistically investigate the extent to which the ratio also varies when moving from the spiral arms into the interarm region at fixed radius, we divided the points into radial bins of width 100″, and within each radial bin, we identified the 10% of points (plotted in red) with the highest spiral arm fraction. The latter was calculated by creating an image of the "spiral-arm fraction" at the resolution of the 170 $\mu$m image using an analogous procedure to that described in § 2. Over the entire radial range, the red points tend to be clustered at the low values of the FIR/UV ratio, meaning that this ratio takes systematically higher values for the diffuse interarm emission than for the spiral-arm emission at a given radius.

## 4. DISCUSSION

To explain our results, we must consider the sources and the propagation of the UV photons within the galaxy and the connection of these to the heating and distribution of the dust grains. Here we consider an approximate analytical treatment of these effects in order to identify the primary reasons for the observed trends. For a more detailed investigation, fully self-consistent radiative transfer techniques would need to be applied, such as those by Bianchi et al. (1996), Ferrara et al. (1999), Baes & Dejonghe (2001), and Tuffs et al. (2004).

In the spiral arm regions, the UV photons originate from young stars embedded in the H II regions. A fraction $F$ of the UV luminosity $L_*$ can be considered to be locally absorbed and reradiated by dust in the vicinity of the H II region, and a fraction $(1 - F)$ escapes the H II region. Thus, we can treat the H II regions as sources in the spiral arms emitting both UV and FIR, with luminosities $(1 - F)L_*$ and $FL_*$, respectively. The factor $F$ is simply a geometrical blocking factor that provides a "gray" attenuation, independent of wavelength. A detailed physical description of the factor $F$ is given in Tuffs et al. (2004).

Having escaped from the H II regions, the UV light emitted

in the direction of the observer (perpendicular to the disk for a face-on system like M101) further passes through a layer of diffuse dust, which also attenuates the UV and augments the FIR. So the FIR and UV luminosity observed along each line of sight will be: $L_{\rm FIR}^{\rm obs,\,arm} = FL_* + (1-F)L_*G$ and $L_{\rm UV}^{\rm obs,\,arm} = (1-F)L_*(1-G)$, where $G$ is the probability of absorption in the layer of diffuse dust for a UV photon traveling perpendicular to the disk. The resulting FIR/UV ratio seen toward the spiral arm regions is then given by

$$\frac{L_{\rm FIR}^{\rm obs,\,arm}}{L_{\rm UV}^{\rm obs,\,arm}} = \frac{[F/(1-F)]+G}{1-G}. \quad (1)$$

The interarm regions are pervaded by diffuse UV light, with relatively few stellar sources (see Bianchi et al. 2005; Thilker et al. 2005a, 2005b). Because of the smooth appearance of the diffuse interarm emission, we will work under the hypothesis that this diffuse interarm UV emission is radiation escaping from the spiral arms, traveling in the plane of the disk, and subsequently being scattered by grains into the observer's line of sight perpendicular to the disk. Thus, we can treat the dust grains scattering the UV light as "sources" in the interarm regions emitting both UV and FIR, with luminosities proportional to $u_{\rm UV}\sigma_{\rm ext}a_{\rm UV}^{\perp}$ and $u_{\rm UV}\sigma_{\rm ext}(1-a_{\rm UV})$, respectively. Here $u_{\rm UV}$ is the local energy density of the UV radiation field, $\sigma_{\rm ext}$ is the extinction cross-section of the grain, $a_{\rm UV}$ is the angle-averaged albedo of the grain, and $a_{\rm UV}^{\perp}$ is the albedo multiplied by the phase function for light scattered at 90°. The UV scattered light traveling toward the observer must then pass perpendicularly through the layer of diffuse dust, which attenuates the UV and augments the FIR. If we also consider that in general some fraction ($\eta$) of the FIR emission will be powered by optical photons, the FIR and UV luminosity observed along each line of sight toward the interarm regions will be $L_{\rm FIR}^{\rm obs,\,inter} \sim [u_{\rm UV}\sigma_{\rm ext}(1-a_{\rm UV}) + u_{\rm UV}\sigma_{\rm ext}a_{\rm UV}^{\perp}G]/[1-\eta]$ and $L_{\rm UV}^{\rm obs,\,inter} \sim u_{\rm UV}\sigma_{\rm ext}a_{\rm UV}^{\perp}(1-G)$. The resulting FIR/UV ratio seen toward the interarm regions is then given by

$$\frac{L_{\rm FIR}^{\rm obs,\,inter}}{L_{\rm UV}^{\rm obs,\,inter}} = \frac{[(1-a_{\rm UV})/a_{\rm UV}^{\perp}]+G}{(1-\eta)(1-G)}. \quad (2)$$

For simplicity, we first make the approximation that $\eta = 0$, in which case equation (1) has the same functional form with respect to $G$ as equation (2). Since there is no reason why $F$ or $a_{\rm UV}$ should depend on radial position, the strong radial dependence seen in Figure 2 can only be attributable to the radial dependence of the factor $G$, the absorption probability for UV photons travelling through the diffuse dust. In other words, our results imply the presence of a large-scale distribution of diffuse dust having a face-on optical depth that decreases with radius and that dominates local variation in opacity between the arm and interarm regions.

For the case of $\eta = 0$, equations (1) and (2) also indicate that the observed systematic difference between the FIR/UV ratio in the arm and interarm regions is attributable to the difference between the factors $F/(1-F)$ (for the arms) and $(1-a_{\rm UV})/a_{\rm UV}^{\perp}$ (for the interarm regions), with the amplitude of the difference also depending on the value of $G$. Using the values of the albedo given by the model of Laor & Draine (1993) and the phase function from Henyey & Greenstein (1941), we obtain $(1-a_{\rm UV})/a_{\rm UV}^{\perp} = 2.98$. Values of typically 0.25 for the $F$ factor have been derived from self-consistent modeling of the UV/FIR/submillimeter spectral energy distributions of normal galaxies (Popescu et al. 2000; Misiriotis et al. 2001), yielding a value of 0.33 for $F/(1-F)$. These values for $F/(1-F)$ and $(1-a_{\rm UV})/a_{\rm UV}^{\perp}$ are consistent with the observed FIR/UV ratio being smaller in the arm than in the interarm region.

For the case of $\eta > 0$, the FIR/UV ratio in the interarm region will be further boosted, because of the expected increase in the fraction of FIR emission powered by optical photons at larger distances from the H II regions in the spiral arms. The combined effect of the optical heating and the scattering of the UV emission means that the FIR/UV ratio will not be a good indicator of extinction in the interarm region. One should also bear in mind that the observed difference in the FIR/UV ratio between the arm and interarm region from Figure 2 is in fact reduced from the prediction of equations (1) and (2) (for any plausible value of $G$) because of beam smearing. Furthermore, even in the most extreme interarm regions, it is apparent from the full-resolution *GALEX* image that some sources of UV emission are present (see Bianchi et al. 2005).

*GALEX* is a NASA small explorer launched in 2003 April. We gratefully acknowledge NASA's support for construction, operation, and science analysis for the *GALEX* mission, developed in cooperation with the Centre National d'Etudes Spatiales of France and the Korean Ministry of Science and Technology.

REFERENCES

Baes, M., & Dejonghe, H. 2001, MNRAS, 326, 733
Bianchi, S., Ferrara, A., & Giovanardi, C. 1996, ApJ, 465, 127
Bianchi, L., et al. 2005, ApJ, 619, L71
Boissier, S., Boselli, A., Buat, V., Donas, J., & Milliard, B. 2004, A&A, 424, 465
Boissier, S., et al. 2005, ApJ, 619, L83
Bothun, G. D., & Rogers, C. 1992, AJ, 103, 1484
Buat, V., et al. 2005, ApJ, 619, L51
Ferrara, A., Bianchi, S., Cimatti, A., & Giovanardi, C. 1999, ApJS, 123, 437
Henyey, L. G., & Greenstein, J. L. 1941, ApJ, 93, 70
Laor, A., & Draine, B. T. 1993, ApJ, 402, 441
Lemke, D., et al. 1996, A&A, 315, L64
Martin, D. C., et al. 2005, ApJ, 619, L1
Misiriotis, A., Popescu, C. C., Tuffs, R. J., & Kylafis, N. D. 2001, A&A, 372, 775
Morrissey, P., et al. 2005, ApJ, 619, L7
Popescu, C. C., Misiriotis A., Kylafis, N. D., Tuffs, R. J., & Fischera, J. 2000, A&A, 362, 138
Popescu, C. C., & Tuffs, R. J. 2002, MNRAS, 335, L41
Popescu, C. C., Tuffs, R. J., Völk, H. J., Pierini, D., & Madore, B. F. 2002, ApJ, 567, 221
Sofue, Y., Tutui, Y., Honma, M., & Tomita, A. 1997, AJ, 114, 2428
Thilker, D., et al. 2005a, ApJ, 619, L67
———. 2005b, ApJ, 619, L79
Tuffs, R. J., & Gabriel, C. 2003, A&A, 410, 1075
Tuffs, R. J., & Popescu, C. C. 2003, in Exploiting the *ISO* Data Archive: Infrared Astronomy in the Internet Age, ed. C. Gry et al. (ESA SP-511; Noordwijk: ESA), 239
Tuffs, R. J., Popescu, C. C., Völk, H. J., Kylafis, N. D., & Dopita, M. A. 2004, A&A, 419, 821
Tuffs, R. J., et al. 2002, ApJS, 139, 37 (erratum 140, 609)
Xu, C., & Buat, V. 1995, A&A, 293, L65